Bioactive Materials 28 (2023) 420–431

Contents lists available at ScienceDirect

Bioactive Materials

journal homepage: www.keaipublishing.com/en/journals/bioactive-materials

One-step fabrication of cell sheet-laden hydrogel for accelerated wound healing

Huijuan Wang [a], Deshun Sun [c], Weiming Lin [d], Chao Fang [d], Kui Cheng [d], Zhengzhou Pan [e], Daping Wang [b,***], Zhangfa Song [a,**], Xiaojun Long [a,b,*]

[a] Department of Colorectal Surgery, Key Laboratory of Biological Treatment of Zhejiang Province, Sir Run Run Shaw Hospital, School of Medicine, Zhejiang University, Hangzhou, Zhejiang, 310016, China
[b] Shenzhen Second People's Hospital, First Affiliated Hospital of Shenzhen University Health Science Center, Shenzhen, 518035, China
[c] Southern University of Science and Technology Hospital, Intelligent Medical Innovation Center, Shenzhen, 518035, China
[d] School of Materials Science and Engineering, State Key Laboratory of Silicon Materials, Cyrus Tang Center for Sensor Materials and Applications, Zhejiang University, Hangzhou, 310027, China
[e] Department of Nuclear Medicine, The First Affiliated Hospital of Zhejiang University School of Medicine, Shenzhen, 518035, China

ARTICLE INFO

Keywords:
Cell sheets
Hydrogel
Full-thickness skin wound
Dermal construction
Cell sheet-laden hydrogel

ABSTRACT

Full-thickness skin wounds are have continued to be reconstructive challenges in dermal and skin appendage regeneration, and skin substitutes are promising tools for addressing these reconstructive procedures. Herein, the one-step fabrication of a cell sheet integrated with a biomimetic hydrogel as a tissue engineered skin for skin wound healing generated in one step is introduced. Briefly, cell sheets with rich extracellular matrix, high cell density, and good cell connections were integrated with biomimetic hydrogel to fabricate gel + human skin fibroblasts (HSFs) sheets and gel + human umbilical vein endothelial cells (HUVECs) sheets in one step for assembly as a cell sheet-laden hydrogel (CSH). The designed biomimetic hydrogel formed with UV crosslinking and ionic crosslinking exhibited unique properties due to the photo-generated aldehyde groups, which were suitable for integrating into the cell sheet, and ionic crosslinking reduced the adhesive force toward the substrate. These properties allowed the gel + cell sheet film to be easily released from the substrate. The cells in the harvested cell sheet maintained excellent viability, proliferation, and definite migration abilities inside the hydrogel. Moreover, the CSH was implanted into a full-thickness skin defects to construct a required dermal matrix and cell microenvironment. The wound closure rate reached 60.00 ± 6.26% on the 2nd day, accelerating mature granulation and dermis formation with skin appendages after 14 days. This project can provide distinct guidance and strategies for the complete repair and regeneration of full-thickness skin defects, and provides a material with great potential for tissue regeneration in clinical applications.

1. Introduction

The high-quality repair of full-thickness skin wounds is a practical topic in clinical and fundamental research, that calls for dermal restoration and skin appendage regeneration [1,2]. The dermis is mainly composed of connective tissue, including collagen fibers, elastic fibers and matrix [3]; more importantly, it pertains to a large number of appendages, such as blood vessels, lymphatics, muscles, hair follicles, sebaceous glands and sweat glands [4,5]. At present, autologous or allogeneic skin transplantation has shown a remarkable therapeutic effects on skin regeneration; however, donor tissue sources are limited, and secondary damage may be caused, and hindering the popularization of this technique [6]. As an alternative for autologous or allogeneic skin, artificial tissue constructs [7]. That contain biological scaffolds and living cells have the advantages of a wide range of sources, moderate price, simple preparation and adjustable physical and chemical

Peer review under responsibility of KeAi Communications Co., Ltd.
* Corresponding author. Department of Colorectal Surgery, Key Laboratory of Biological Treatment of Zhejiang Province, Sir Run Run Shaw Hospital, School of Medicine, Zhejiang University, Hangzhou, Zhejiang, 310016, China.
** Corresponding author.
*** Corresponding author.
E-mail address: 11726067@zju.edu.cn (X. Long).

https://doi.org/10.1016/j.bioactmat.2023.06.005
Received 11 December 2022; Received in revised form 12 May 2023; Accepted 7 June 2023
Available online 20 June 2023

properties, endowing them with great application potential of use in skin barriers, wound healing, skin reconstruction, and skin accessory regeneration [8,9].

Biomimetic hydrogel materials are well suited for use as scaffolds for artificial tissue constructs [10,11]. In particular, biomimetic hydrogels have the advantages of superior biocompatibility, biodegradability, and low immunogenicity and can provide a suitable three-dimensional (3D) network structure, mechanical support, moist microenvironment, and skin-like composition for skin regeneration [12,13]. Various designed hydrogels, such as photocurable gelatin methacryloyl (GelMA)/poly (ethylene glycol) diacrylate (PEGDA) [14], GelMA/N-(2-aminoethyl)-4-(4-(hydroxymethyl)-2-methoxy-5-nitro-sophenoxy) butanamide (NB)-linked hyaluronic acid (HA-NB) [6], and polyurethane (PU)/gelatin [15], have been applied as tissue scaffolds to encapsulate specific skin-associated cells, such as skin fibroblasts, umbilical vein endothelial cells, and keratinocytes, and were assembled as a tissue constructs [15–17]. However, most cells are acquired by trypsin digestion, and the contact between cells is destroyed in this process, which affects affecting the activity and specific functions of cells [18].

In recent years, cell sheet technology has been widely used in the field of tissue engineering because of its advantages of retaining high-density cell tissue and the natural ECM secreted by cells, and the ability to be engineered and has thus been explored as a promising solution for skin repair, scar reduction, and even perfect regeneration [19,20]. For example, oral mucosal and skin cell sheets can promote wound healing with early wound closure and less scarring [21], multilayer adipose-derived stem cells can be a potentially viable matrix for full-thickness defect wound healing in a mouse model [22], and spheroid-incorporated human dermal fibroblast sheets can mediate the activity of inflammatory cytokines for M2 polarization and increase angiogenic efficacy for wound healing [23]. Currently, the most widely known cell sheet harvesting technologies are realized by regulating the reaction between the intelligent interface of the cell sheet and thermo-responsive [24], photo-responsive [25], magnetic-responsive [26], or electro-responsive biomaterials [27]. However, scaffold-free cell sheets lack sufficient mechanical performance and cell viability, crimping, wrinkling and destruction of the cell sheet are inevitable, all of which limit their application for skin regeneration. Considering these aspects, the integration of scaffolds with cell sheets for high overall performance is an extremely promising strategy [28].

Therefore, in this work, cell sheets were harvested and integrated with a biomimetic hydrogel through a one-step strategy, and rapidly assembled to form a cell sheet-laden hydrogel (CSH) by layer-by-layer superposition, simulating the function of the epidermis and dermis in the skin. As Fig. 1 shows, the biomimetic hydrogel introduced in our previous work was prepared by incorporating GelMA, N-(2-aminoethyl)-4-(4-(hydroxymethyl)-2-methoxy-5-nitro-sophenoxy) butanamide (NB)-linked sodium alginate (Alg-NB), and the photoinitiator lithium phenyl-2,4,6-trimethylbenzoylphosphinate (LAP). The GelMA/Alg-NB/LAP (G-A) hydrogel was formed through both UV crosslinking and ionic crosslinking, which gave the hydrogel strong mechanical properties, strong adhesion to wet tissue and slow degradation characteristics [29]. Moreover, the human skin fibroblast (HSFs sheet and human umbilical vein endothelial cell (HUVEC) sheet were obtained by *in vitro* culture and were integrated with the prepared pre-gel. Then, the G-A hydrogel was formed in situ by photo-crosslinking and ionic crosslinking and overlapped as a double layer of CSH composite film. The activities of the cell sheets and their interactions with the hydrogel were investigated via *in vitro* measurements. Finally, a full-thickness defect Sprague-Dawley (SD) rat model was constructed, and CSH was adhered to the defect with the help of the G-A hydrogel via in situ gelling. The effect and mechanism of full-thickness wound healing by CSH were evaluated by hematoxylin–eosin (H&E) staining, Masson's trichrome (MT) staining, and immunohistochemical staining.

2. Methods and materials

2.1. Synthesis of biomimetic hydrogel

The preparation of the biomimetic hydrogel with a triple-network

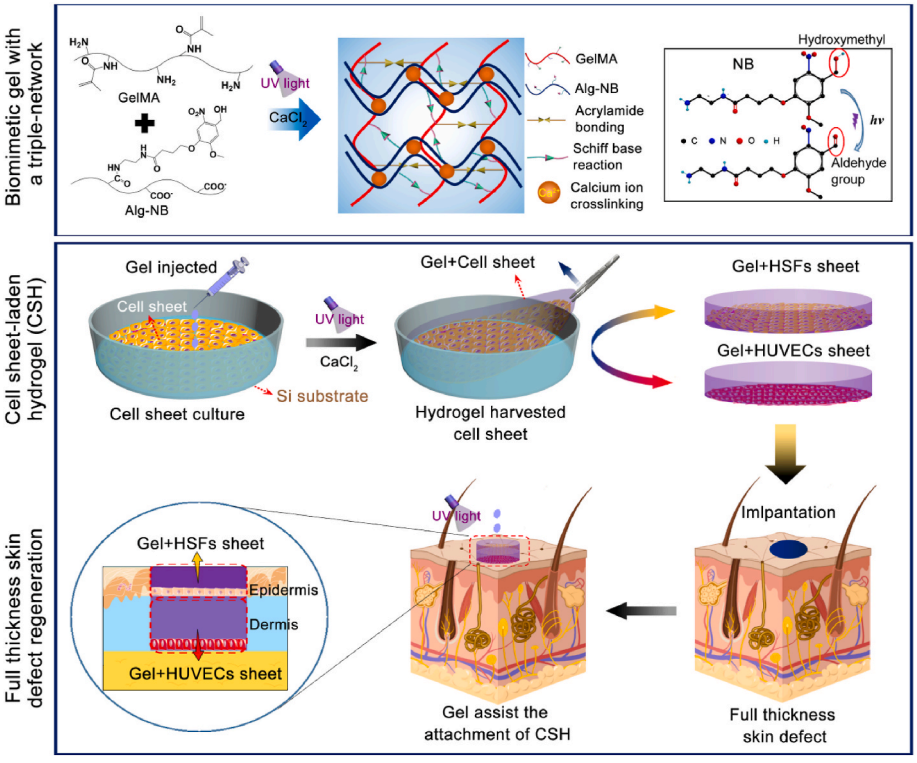

Fig. 1. Schematic illustration of the formation of the biomimetic gel with a triple-network, the preparation of the cell sheet-laden hydrogel (CSH), and application of the CSH for full-thickness skin regeneration.

structure was described in our published paper [29], and the synthesis method is briefly described here. First, methacrylic anhydride (MA) (Sigma-Aldrich) was grafted with gelatin (Sigma-Aldrich) to obtain GelMA, and alginate (Alg) (Aladdin Chemical Reagent, molecular weights (Mw) of approximately 20,000–50,000, M/G units of approximately 1:2) was grafted with UV-light-sensitive N-(2-aminoethyl)-4-(4-(hydroxymethyl)-2–methoxy-5-nitro-sophenoxy) butanamide (NB) (Haining Jurassic Biotechnology Co., Ltd.) to obtain Alg-NB. Then, GelMA, Alg-NB, and the polymerization initiator lithium phenyl-2,4,6-trimethylbenzoylphosphinate (LAP) (Haining Jurassic Biotechnology Co., Ltd.) were mixed in PBS to prepare glue solutions, and the concentrations of GelMA, Alg-NB, and LAP were set as 5 wt%, 1 wt%, and 0.1 wt%, respectively. Finally, ultraviolet (UV) light (365 nm, 30 mW/cm^2) was applied for UV crosslinking (to form the G-A-l hydrogel) and $CaCl_2$ solution was used for calcium ion crosslinking (to form the G-A-l-i hydrogel, or abbreviated as G-A).

2.2. Rheological studies

The rheological properties of the GelMA/LAP, GelMA/Alg-NB, and GelMA/Alg-NB/LAP hydrogels were evaluated to determine their UV light crosslinking characteristics and mechanical properties, and a photorheometer with a parallel-plate (Discovery HR-3, TA, USA) geometry and an OmniCure Series 2000 (365 nm, 30 mW/cm^2) at 37 °C were used to determine the rheological properties of the hydrogels. The tested time was set to 180 s. The gel point was defined as the time at which the torsion modulus (G′) surpassed the loss modulus (G″).

2.3. Cell culture

Human skin fibroblast cells (HSFs) were cultured on PS dishes in Dulbecco's modified Eagle's medium (DMEM; CellMax) supplemented with 10% fetal bovine serum (FBS, CellMax) and 1% antibiotic solution containing 10,000 units/mL penicillin, and 10,000 mg/mL streptomycin (CellMax). Then, the cells were incubated in a humidified atmosphere with 5% CO_2 at 37 °C. The cultured cells were harvested with 0.25% trypsin/EDTA (CellMax) and suspended in fresh culture media for the next subsequent subculture experiments. The same method was performed for the culture of human umbilical vein endothelial cells (HUVECs). HSFs and HUVECs were purchased from the American Type Culture Collection (ATCC, USA).

2.4. Cytocompatibility of the hydrogels

HSFs and HUVECs were used to assess the cytocompatibility of the hydrogels. First, GelMA/LAP (G) and G-A hydrogels were submerged in culture medium for 24 h to obtain an extraction medium (Fig. 2a), which contained a mixture of the extract of the hydrogels and culture medium. Then, cells (20000 cells/mL gel) were seeded on PS dishes with the prepared extraction medium and incubated in a humidified atmosphere with 5% CO_2 at 37 °C. Finally, after 1, 3 and 5 days of culture, the activity of the cells in the hydrogels was detected by a cell counting kit-8 (CCK-8), using normal medium as a control.

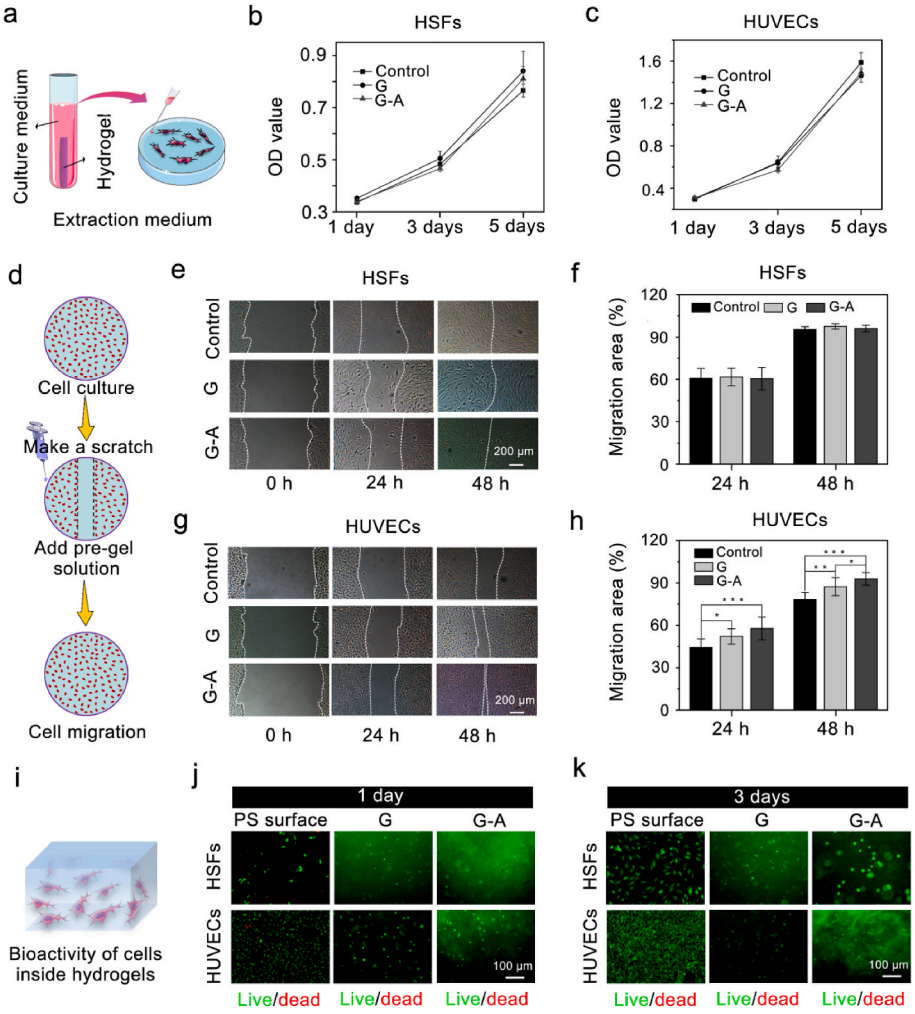

Fig. 2. Cytocompatibility, cell migration properties, and cellular bioactivity of the G-A hydrogel. (a) Schematic diagram of the preparation process for the hydrogel extraction medium, and the cytocompatibility was measured with the CCK-8 assay after (b) HSFs and (c) HUVECs were cultured in the extraction medium of G and G-A hydrogels for 1, 3, and 5 days, respectively, and the normal medium was set as the control group; (d) Schematic diagram of the scratch assay. Scratch assay images of HSFs (e,f) and HUVECs (g,h) migration into the scratched area cultivated with G and G-A pre-gel solution treated samples. Scale bars: 200 μm; (i) Schematic diagram of cell encapsulation in the hydrogel. Live/dead staining of HSFs and HUVECs encapsulated in G and G-A hydrogels and cultured for 1 day (j) and 3 days (k), where the calcein AM indicates live cells (green) and ethidium homodimer-1 indicates dead cells (red), the PS substrate was used as a control group. Scale bars: 100 μm. (*$p < 0.05$, **$p < 0.01$, ***$p < 0.001$; $n = 4$ each experimental/study group; Student's *t*-test).

2.5. Cell migration

The effects of the hydrogels on the migration efficiency of HSFs and HUVECs were measured by a cell scratch assay. As Fig. 2d shows, the cells were first seeded into a 24-well plate (5000 cells/cm^2) and cultured until the cells fully covered the surface. Then, a straight cell scratch was gently created, and the cells were washed twice with PBS. Next, 100 μL of G-A pre-gel solution was added to the medium. The migration efficiency of the cells was observed by optical microscopy after 24 h and 48 h of culture. The PS culture plate and G group (GelMA/LAP) were used as the control groups.

2.6. Bioactivity of cells inside the hydrogels

The viability of the cells in the hydrogels was determined by a live-dead cell staining kit (Abnova). First, HSFs/HUVECs were uniformly suspended in a sterile G-A hydrogel precursor solution and added dropwise to culture dishes. Then, UV crosslinking and calcium ion crosslinking were performed to achieve the in situ gelation of the hydrogels. Next, Dulbecco's modified Eagle's medium was added, and the samples were incubated in a humidified atmosphere with 5% CO_2 at 37 °C. Finally, after 1 and 3 days of culture, a live-dead cell staining kit (Abnova) was used to measure the cell viabilities of the cells in the hydrogels. The uptake of fluorescent indicators was detected using a confocal microscope. Cells encapsulated in the G hydrogel were used as a control group.

2.7. The ability of hydrgels to support angiogenesis

The ability of the hydrogels to support HUVEC angiogenesis for hydrogel was evaluated with tube formation assays. First, 330 μL of G hydrogel, G-A hydrogel, and matrix glue (Corning, 354262) were added to 24-well plates. Then, HUVECs ($1*10^5$ cells/cm^2) cultured in DMEM medium were seeded on the surface of the G hydrogel, the G-A hydrlgel, and matrix glue and incubated in a humidified atmosphere with 5% CO_2 at 37 °C. Finally, after 12 h of culture, calcein staining was carried out to examine to measure the cell morphology, and fluorescent indicators were detected using a confocal microscope. The PS surface was used in the negative control group, and Matrigel was used in the positive control group.

2.8. Preparation of CSH

The methods by which the cell sheets were cultured and tested for activity were as follows. First, the surface-polished silicon (Si) substrate (undoped, diameter of 10 mm, thickness of 150 μm), which was designed to match the size and shape of the wound and has a clear and smooth surface for harvesting the CSH, was autoclaved. Then, HSFs and HUVECs were seeded on the surface of the Si substrate at a density of 1×10^5 cells/cm^2 and cultured for 3 days to obtain HSF and HUVEC sheets. The bioactivity of the cell sheets was determined by a live-dead cell staining kit.

Assembly of the hydrogel harvested cell sheets as CSH. After HSF sheets and HUVEC sheets were obtained on the surface of the Si substrate, G-A pre-gel solution was dropped onto the surface of the cell sheet/Si. The amount of pre-gel solution needed was determined by the size of the skin defect in the subsequent full-thickness skin defect model. After 30 s of UV illumination at 365 nm (30 mW/cm^2) and the addition of an excess of $CaCl_2$ solution to complete the ionic crosslinking, the gel + cell sheet composite films were assembled. Then, the $CaCl_2$ solution was aspirated and PBS solution was added. Finally, the gel + cell sheet films were gently peeled from the surface of the Si substrate and kept in the medium for the next experiments. The bioactivity of the harvested cell sheets inside the hydrogels was detected by a live-dead cell staining kit.

To examine the desorption process of the "gel + cell sheet" films from the Si surface, the G-A-l hydrogel and G-A hydrogel were used to harvest the cell sheets, and this process was video recorded. The static water contact angles of the G, G-A-l, and G-A hydrogels and various Si surfaces were measured with a contact angle meter (Dataphysics, OCA20). The roughnesses of the surface for Si, the G-A gel detached Si, and the G-A gel + cell sheet detached Si were measured by atomic force microscopy (AFM; NTEGRA Spectra, NTMDT). The surface morphologies of Si and the G-A gel + cell sheet detached Si were characterized by scanning electron microscopy (SEM, with an operating voltage of 3.0 kV (Hitachi, SU47)). Energy spectrum analyses were also carried out.

2.9. Cell proliferation and migration assay of the cell sheets inside the hydrogel

After the gel + HSF sheet and gel + HUVEC sheet composite films were detached from the Si substrate, they were transferred were transplanted to a 24-well plate, and 500 μL of medium was added, and cultured for 1, and 5 days of culture. The cell sheets were placed on the upper faces of the gel + cell sheet films. To investigate whether the hydrogel provided a suitable microenvironment for cell proliferation and migration, 4′, 6-diamidino-2-phenylindole (DAPI, ENZ-52404, Enzo Life Sciences, Switzerland) and calcein-AM dye were used to visualize the cells, which were imaged with a laser scanning confocal microscope ((Zeiss LSM 780, Germany).

2.10. In vivo full-thickness skin defect healing experiments

To investigate the wound healing properties of CSH *in vivo*, full-thickness skin defects were created on the dorsal surface of SD rats. First, the 5-week-old male SD rats (approximately 150g) were purchased from the Shanghai Institute of Experimental Animals, Chinese Academy of Sciences, and all the rats were reared in a specific pathogen free (SPF) animal lab with constant temperature, stable relative humidity and pressure gradient. After the SD rats were anesthetized with isoflurane in a sterile environment, a part of the dorsal area of the SD rat was selected for hair removal, and the shaved skin was cleaned and sterilized with 2% povidone–iodine solution. Then, a full-thickness dorsal skin wound model (a circle with a diameter of approximately 10 mm) was made with surgical scissors. Next, CSH was implanted into the full-thickness skin defect area, and G-A hydrogel was injected and formed in situ to assist in its attachment of CSH (Fig. 6a). CSH was assembled by overlaying the gel + HSF sheet (upper) and gel + HUVEC sheet (lower), with placemen of the cell sheets on the bottom side of the gel + cell sheet film. Moreover, the groups of gel (in situ gelling), scaffold (hydrogel colloid column), and gel + cells (layered HSFs and HUVECs dipped in gel) were also applied, and the scaffold and gel + cells were all implanted with the help of G-A hydrogel adhesion. The group without any treatment was set as a blank control. Finally, the process of wound healing was followed by imaging and quantitatively analyzed using ImageJ 1.45 software. At designated time points (2, 6, 10, and 14 days), the rats were euthanized with an overdose of isoflurane, and H&E, Masson trichromatic staining, and immunofluorescence staining (CD31, CD68, α-SMA, and TNF-α) were carried out for histological analysis.

2.11. Study approval

All the animal experiments were approved by the Ethics Committee of Sir Run Shaw Hospital, Zhejiang University.

2.12. Statistical analysis

The sample size and number of animals in each experimental/study group for each experimental measurement was $n = 4$, and the data are expressed as the means ± standard deviations (SDs). Statistical analysis was evaluated via Tukey's post hoc test and one-way analysis of variance. Student's *t*-test was performed by SPSS software, and $*p < 0.05$,

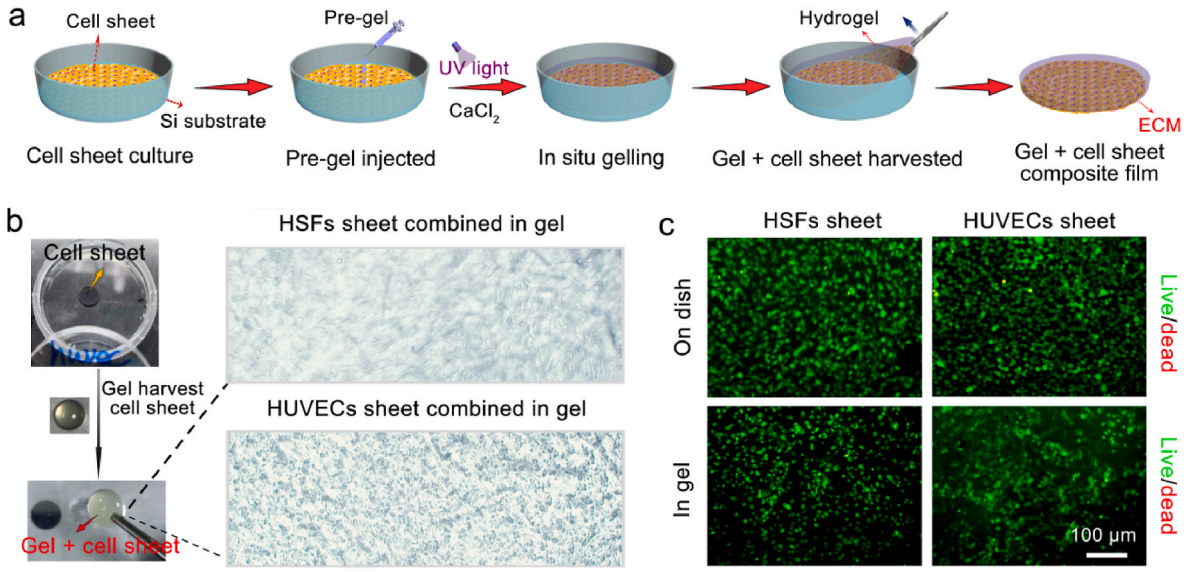

Fig. 3. Hydrogel harvested cell sheet and assembly of the gel + cell sheet composite film. (a) Schematic diagram of the preparation process of the gel + cell sheet composite film; (b) HSFs sheet and HUVECs sheet combined in the G-A hydrogel; (c) Live/dead staining of the HSFs sheet and HUVECs sheet formed on a dish and harvested in G-A hydrogel.

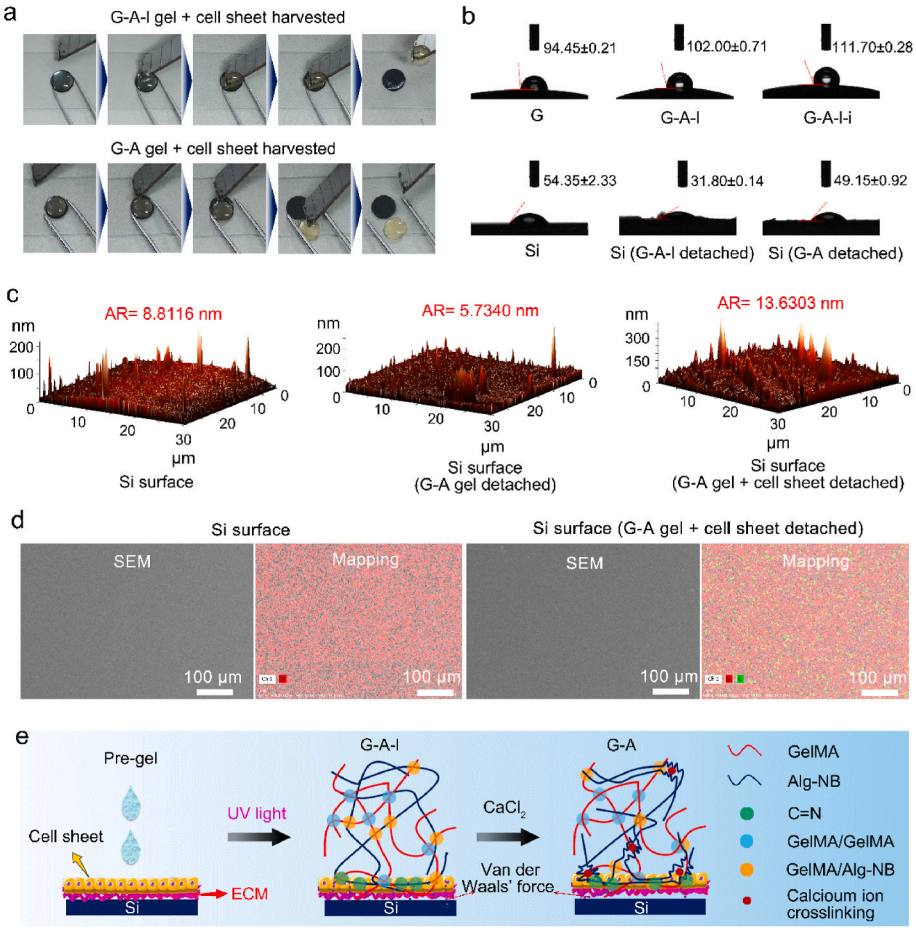

Fig. 4. Cell sheet harvested by G-A hydrogel and the possible corresponding mechanism. (a) Videos of the cell sheet harvesting process by G-A-l and G-A-l-i hydrogels; (b) Contact angles of G hydrogel, G-A-l hydrogel, G-A-l-i hydrogel, Si, Si (G-A-l detached), and Si (G-A-l-i detached); (c) AFM images of the surfaces of Si, G-A gel detached Si, and G-A gel + cell sheet detached Si; (d) SEM images and mapping of the surfaces of Si, and G-A gel + cell sheet detached Si, red marks the Si element and green marks the C element; (e) Schematic diagram of the mechanism of the cell sheet harvesting from the Si surface by the G-A hydrogel.

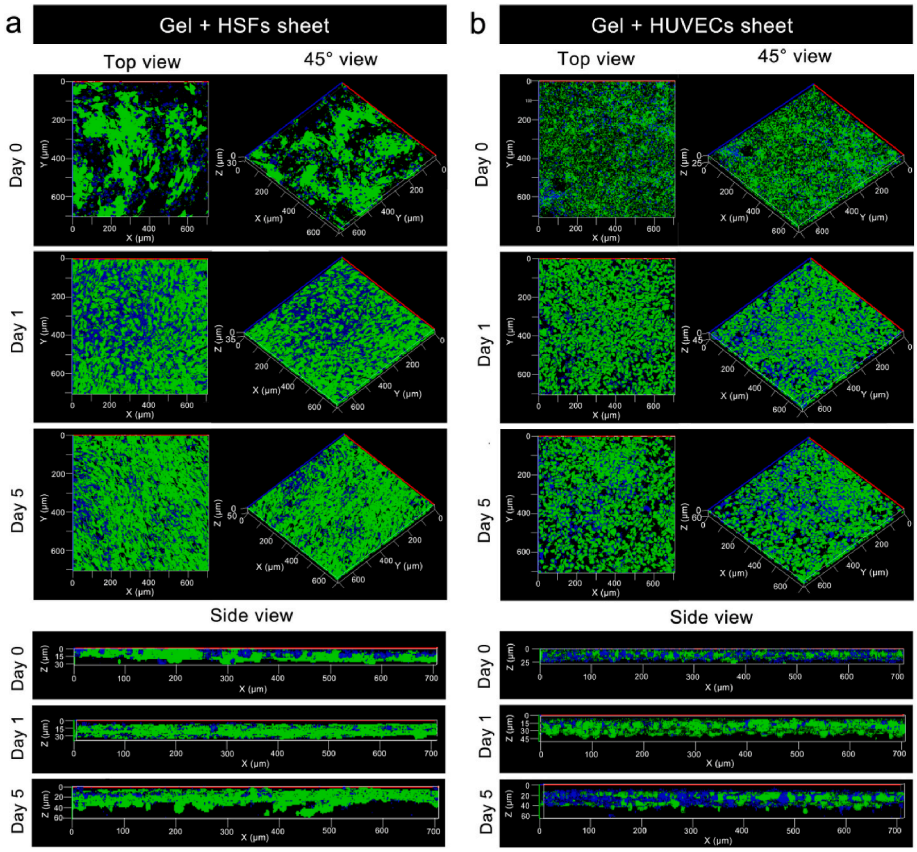

Fig. 5. Analysis of the cell proliferation and migration abilities of cell sheets harvested in hydrogels. (a) Calcein (green) and DAPI (blue) nuclear staining at 0^{th} day, 1st day, and 5th days after HSFs sheets harvested in hydrogel, in order to obtain a HSFs sheets with a high cell density, HSFs were seeded on the surface of the Si substrate at a density of 2×10^5 cells/cm^2 and cultured for 3 days to obtain HSFs sheet, laser scanning confocal microscopy was carried out to determine the morphology of the cell sheet from the top view, 45° view, and side view; (b) Calcein (green) and DAPI (blue) nuclear staining of the HUVECs sheets in the hydrogel at 0^{th} day, 1st day, and 5th days, HUVECs were seeded on the surface of the Si substrate at a density of 1×10^5 cells/cm^2 and cultured for 3 days to obtain HUVECs sheet.

$^{**}p < 0.01$ and $^{***}p < 0.001$ were considered to indicate statistical significance, while NS indicates that there was no significant difference.

3. Results and discussion

3.1. *In vitro evaluation of the bioactivity of the G and G-A hydrogels*

The G-A hydrogel was fabricated with MA-grafted gelatin (GelMA) and NB-linked sodium alginate (Alg-NB). Although the biocompatibility of the G-A hydrogel was demonstrated in our previously published work [29], it is still necessary to demonstrate its influence on cell proliferation, migration and viability for the synthesis of the G-A hydrogel, as the G-A hydrogel was designed to integrate HSF sheets and HUVEC sheets. To evaluate the biocompatibility of the G and G-A hydrogels with HSFs and HUVECs, cell proliferation was assessed using the CCK-8 assay at 1 day, 3 days, and 5 days, respectively. As Fig. 2a–c shows, cell proliferation in both hydrogels increased with time, indicating the excellent biocompatibility of the G-A hydrogel.

After the cell sheets were integrated into hydrogels, a superior promotion of the cell migration ability of the hydrogels would be helpful for cell sheets to migrate into the hydrogel [30,31]. Therefore, a cell migration test was used to determine whether the G-A hydrogel could promote cell migration. For the case of the HSFs, no significant cell migration promotion effect was observed with the G and G-A hydrogels, compared that obtained for the control group without the addition of pre-gel (Fig. 2 e,f). However, the G and G-A hydrogels both showed potential promotion effects on cell migration for HUVECs, and G-A exhibited a more effective cell migration promotion effect (Fig. 2 g,h). As the HSFs has a superior migration ability in various condition, the signaling molecules provided by hydrogel may can be ignored. However, the adhesion and migration ability for the HUVECs are relatively lower than the HSFs, the signaling molecules provided by hydrogel may play a significantly role. Therefore, that is the most possible reason for why G and G-A hydrogels failed to facilitate the migration of HSFs but facilitated the migration of HUVECs. Moreover, the HUVECs on the surface of G-A hydrogel exhibit the phenomenon of polarity distribution, indicating its potential to support angiogenesis (Fig. S1). These result suggested that the G-A hydrogel might enhance integrated cell sheet migration and recruit more cells *in vivo*.

Next, the cell viability of the cells inside the hydrogels was verified through the Live/dead staining. As Fig. 2 j and k shows, the HSFs and HUVECs both maintained excellent cell viability inside the G and G-A hydrogels, compared with the cells cultured on the surface of the PS substrate.

All these results demonstrated that the G-A hydrogel has superior biocompatibility, and can promote HUVEC migration, indicating that the G-A hydrogel is a qualified candidate for combined cell sheets and to form a "gel + cells sheet" film.

3.2. *One-step fabrication of the "gel + cell sheet" film*

The preparation process of the "gel + cell sheet" film is shown in Fig. 3a. After HSFs or HUVECs were cultivated to form a cell sheet on the surface of the Si substrate, the G-A pre-gel solution was injected and integrated with the cell sheet, and the G-A hydrogel formed in situ with UV crosslinking and ionic crosslinking. Then, the combined "gel + cell sheet" film was detached from the Si substrate, and the one-step fabrication process of harvesting the cell sheet and integrating cell sheet into the hydrogel to form a "gel + cell sheet" film was realized at the same time. As Fig. 2b shows, through the one-step fabrication strategy, HSFs sheet and HUVECs sheet could combine in the G-A hydrogel, respectively. Moreover, according to the live/dead staining test results, the integrated HSFs and HUVECs maintained an excellent viability inside the hydrogel (Fig. 3c). This result indicates the successful fabrication of the gel + cell sheet film, and provided superior cell viability. The retained cell viability of the cell sheet indicated that this one-step

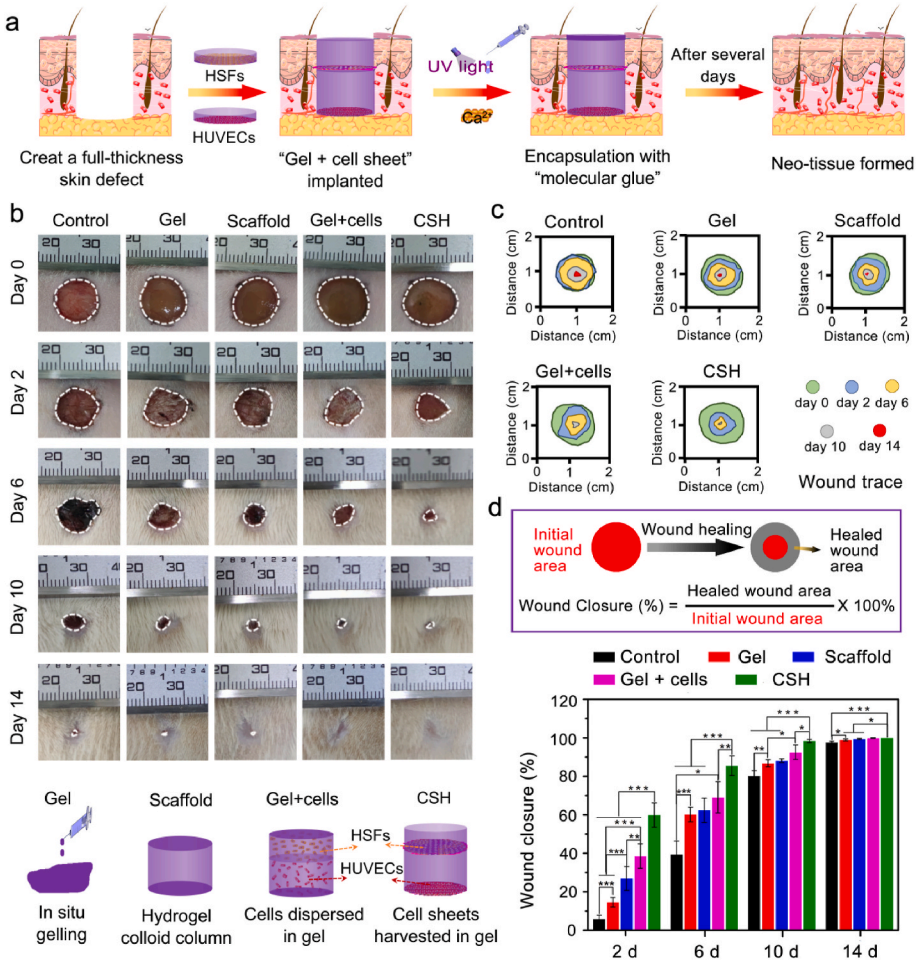

Fig. 6. CSH for full-thickness skin defect repair in a rat model. (a) Schematic representation of the surgical process. Full-thickness defects were created on the dorsal surface of SD rats, and the G-A hydrogel was injected and formed in situ to assist in its attachment of CSH. The CSH was assembled through the overlaying of the "gel + HSFs sheet" (upper) and "gel + HUVECs sheet" (lower); **(b)** Representative photographic images of wounds at 2, 6, 10 and 14 days for treatment with gel (in situ gelling), scaffold (hydrogel colloid column), "gel + cells" (HSFs and HUVECs layered dipped in gel), and CSH, respectively. The untreated group functioned as the control group; (c) Traces of wound-bed closure during 14 days for each treatment; (d) Calculation method of wound closure, and percentage of wound closure for each treatment on days 2, 6, 10 and 14 post-operation, (*$p < 0.05$, **$p < 0.01$, ***$p < 0.001$; $n = 4$ each experimental/study group; Student's *t*-test).

fabrication strategy is a noninvasive process for [32].

Moreover, we examined how the G-A hydrogel could integrate into the cell sheet and be released from the Si surface. As our previous published paper proved, the G-A hydrogel is a biomimetic hydrogel with a triple-network attained through UV crosslinking and ionic crosslinking, that exhibited mechanical properties superior to those of the G and G-A-l hydrogels (Fig. S2) [29]. The adjustable mechanical properties of the G-A hydrogel allowed the cell sheet to be supported [19], and the cell sheet was not easily broken through the cell sheet harvesting process. More significantly, the adhesion force of the hydrogel toward the substrate could determine the cell sheet harvesting efficiency [33], and surface polished Si with a smooth surface was designed as a culture substrate for the cell sheet. As Fig. 4a shows, regarding the harvesting effect of the G-A-l gel + cell sheet, the G-A gel + cell sheet could be released from the Si surface more easily (Movie S1, and Movie S2); in fact, the adhesion force between the G-A hydrogel and Si was too small to be detected by a conventional uniaxial testing machine.

Supplementary video related to this article can be found at https://doi.org/10.1016/j.bioactmat.2023.06.005

The G-A hydrogel formed through UV crosslinking and ionic crosslinking with a triple-network compared with the G hydrogel formed with a single network [34] and the G-A-l hydrogel formed with a double-network, and the G-A hydrogel displayed superior mechanical properties [29]. More importantly, the G-A hydrogel had superior hydrophobic surface characteristics, the water contact angle on the surface of the G-A hydrogel increased to $111.70 \pm 0.28°$, compared with results of $94.45 \pm 0.21°$ for the G hydrogel, and $102.00 \pm 0.71°$ for the G-A-l hydrogel (Fig. 4b). As most hydrogels have the characteristics of an internal porous structure and high water content [35,36], hydrogels are internally hydrophilic [37], however, on the surface of the hydrogels, rough and non-porous structures were observed (Fig. S3), which may be the reason why the G-A hydrogel had superior hydrophobic surface characteristic [38]. The high mechanical strength and super surface hydrophobic characteristics of the G-A hydrogel might be the reason why the G-A gel + cell sheet was released from the surface of the Si substrate more easily. Moreover, as indicated by the results of the water contact angle test and AFM measurements, the Si surface after G-A gel detachment had less residue than the Si surface after G-A-l gel detachment, and Si surface after G-A gel + cell sheet detachment was clear (Fig. 4b and c). In addition, the results of SEM and the mapping tests showed that the Si surface after G-A gel + cell sheet detachment had no visible residue, and the presence of carbon which can be monitored by mapping tests, might be due to some inevitable trace residues from the hydrogel or ECM (Fig. 4d). All these results indicated that the G-A hydrogel was a suitable candidate for use as a cell sheet integration scaffold. As a photo-responsive molecule, the grafted NB in the G-A hydrogel can generate aldehyde groups [39], which would be beneficial for anchoring the amidogen on the cell sheet [40]. Moreover, ionic crosslinking could increase the hydrophobic surface characteristics, shrinking the colloid and decreasing the adhesion force toward the Si surface. These are the most likely reasons why the G-A hydrogel could integrate into the cell sheet and easily detached from the Si surface (Fig. 4e).

3.3. Evaluation of the cell sheet proliferation and migration abilities within the hydrogels

After the cell sheets were harvested with the hydrogels, the

proliferation and migration abilities of the cells in the hydrogel also need to be determined [6,13], as these properties are fundamentally crucial for their further application of in skin repair and regeneration. As the results of day 0 in Fig. 5 show, HSFs sheet and HUVECs sheet could be harvested by the G-A gel. Moreover, the harvested cell sheets maintained a complete lamellar structure in the gel, the morphologies of the HSFs and HUVECs maintained their typical shuttle and elliptical structures [41,42], respectively, and the characteristics of good intercellular connections were preserved, which indicated that the cell sheet could integrate with the G-A hydrogel while maintaining a good morphology and function of the cell sheet. From day 0 to day 5, for the HSFs sheet, the cell proliferation was obvious (top view and 45° view), but no obvious migration was observed in three-dimensional space (side view) (Fig. S4). This phenomenon might contribute to the HSFs sheet having a relatively low cell proliferation ability and low cell density, and cells tend to proliferate and migrate in two-dimensional space. When increasing the number and density of the HSFs sheet by doubling the density of seeded cells on the surface of Si substrate, and the harvested HSFs sheet had a significantly cell density. The thickness of the cell sheet increased from 30 μm (day 0) to 35 μm (day 1) and 60 μm (day 5), indicating the HSFs would migrate into the hydrogel (Fig. 5a). Moreover, for the HUVECs sheet, cell proliferation was obvious (top view and 45° view), and the thickness of the cell sheet increased from 25 μm (day 0) to 45 μm (day 1) and 60 μm (day 5), indicating that HUVECs could migrate inside the hydrogel in three-dimensional space (side view) (Fig. 5b). The possible reason for this could be the high cell density of the HUVECs sheet, and the elliptical structure of the HUVECs allowed them to migrate in the G-A hydrogel more easily. These results all demonstrated that the cells in cell sheet could migrate in three-dimensional space, which is significantly important for its usage *in vivo*.

3.4. *In vivo full-thickness skin repair using CSH*

Finally, the therapeutic effect of the CSH system on skin regeneration was determined by employing it in an SD rat full-thickness dorsal skin defect model (Fig. 6). The skin wound repair schematic diagram is shown in Fig. 6a. After a full-thickness skin defect (a diameter of approximately 1 cm) was created on the dorsal surface of the SD mouse and the CSH was implanted in the defect area, and G-A hydrogel was added to assist the attachment of CSH, the CSH was assembled by overlaying the "gel + HSFs sheet" (upper) and "gel + HUVECs sheet" (lower). Granulation tissue and neo-skin formed after several days. Five groups were used for the wound closure assay were prepared as follows: blank control (untreated), gel (in situ gelling), scaffold (hydrogel colloid column), gel + cells (layered HSFs and HUVECs dipped in gel), and CSH.

The full-thickness skin wound closure process was monitored photographically on days 0, 2, 6, 10, and 14 post-surgery (Fig. 6b). Gross observation of the wound size showed that a remarkable wound closure effect was observed in all treated groups, especially within 6 days, compared with the slow wound closure effect observed in the blank control group during the experimental time. More significantly, hydrogel application resulted in quick closure of the wound, preventing further bleeding and potential bacterial infections (Fig. S5) [10]. Among the treated groups, the gel + cells group possessed a more efficient healing with complete wound closure than the gel and scaffold groups, indicating that the addition of HSFs and HUVECs had a positive effect on wound healing. Moreover, the CSH group exhibited the most efficient healing effect with smooth neo-skin and hair growth at day 14. This result indicated that the cell sheet in CSH could accelerate full-thickness skin wound healing. Consistent with the gross observations, the quantitative analysis of the wound closure rates showed that the CSH produced the fastest closure rate than the other groups throughout the healing process. The wound closure rate reached 60.00 ± 6.26% in the CSH group on the 2nd day, while the other groups reached healing rates of 38.52 ± 6.32% (gel + cells), 26.92 ± 6.14% (scaffold), 14.59 ± 2.49% (gel), and 5.83 ± 1.96% (control). Surprisingly, the wound closure rates for the CSH group reached 85.52 ± 5.08%, 98.37 ± 0.82%, and 100% on the 6th day, 10th day, and 14th day, respectively, which were all significantly higher than those of the other groups at the same times pionts. The most possible mechanism for the 60% wound closure in the CSH group by day 2 was "gel + cell sheet" induced more wound contraction, and the rat skin wound healing/closure is characterized by a mechanism of wound contraction due to its unique skin anatomy. All these results indicated that CSH can accelerate the full-thickness skin defect healing process through the strategy of integrating the G-A hydrogel with a cell sheet, and overlaying the gel + cell sheet to simulate the function of the epidermis and dermis in the skin.

Subsequently, hematoxylin–eosin (H&E) staining was used to evaluate the pathological characteristics of the formed neotissue on the 2nd and 10th days. As shown in Fig. S6a and Fig. 7a, the macroscopic H&E staining images showed that the granulation tissue contained some growth factors, abundant fibroblasts, and accumulated extracellular matrix that filled the wound on the 2nd day and 10th day for all the groups, and gradually formed neo-dermis tissue. In addition, the granulation tissue thickness and length of the wound were also limiting factors for assessing the therapeutic effect of the wound dressing [43], and these parameters were measured with Image-J software. As shown in Figs. S6c and d and Fig. 7c,e, the granulation tissue thicknesses of all the treated groups were significantly thicker and the lengths of the wound were shorter than those of the untreated control group on the 2nd and 10th days. Moreover, the epidermal layer thickness of all the treated groups were also higher than the control group on the 10th days (Fig. 7d). The CSH group with cell sheets showed thicker granulation tissue than that in the gel + cell ($p < 0.05$), scaffold ($p < 0.01$), gel ($p < 0.01$), and control ($p < 0.001$) groups on the 10th day. Moreover, the wounds of the CSH-treated group exhibited the shortest lengths compared with those of the gel + cell ($p < 0.05$), scaffold ($p < 0.001$), gel ($p < 0.001$), and control ($p < 0.001$) groups on the 10th day. It's worth noting that, there was no obvious epithelization on the 2nd day (Fig. S6a) and the wound length data on the 10th day (Fig. 7a,e) could be a good evidence of wound contraction (Fig. 6b,d), more wound contraction and accelerate neo-tissue formation could be the most possible mechanism for CSH promote wound closure. These results further demonstrated that CSH with cell sheets could accelerate full-thickness skin defect repairs efficiently.

Likewise, regarding the Masson's trichrome (MT) staining results, the treated groups and untreated control group exhibited similar granulation tissue thicknesses and wound lengths to those recorded in the results of H&E staining (Fig. S6b, Fig. 7b). Moreover, the content and distribution of collagen fiber in granulation tissue and neo-dermis tissue can be assessed by MT staining [44], and are important factors when evaluating the quality of regenerated skin. On the 2nd day, obvious collagen fibers were visible in the treated groups but significantly decreased in the control group, and the wounds of the CSH-treated group exhibited the highest collagen fraction compared with those of the gel + cell ($p < 0.001$), scaffold ($p < 0.001$), gel ($p < 0.001$), and control ($p < 0.001$) groups on the 10th day (Fig. S6e). On the 10th day, the collagen fibers were more distinctly observed in all the groups. According to the quantitative analysis, the collagen fraction of the CSH group was still the highest of all the treatment groups (Fig. 7e). In addition, capillary vessels and hair follicles were visible in the granulation tissue and neo-dermis tissue for all the groups on the 10th day, and were particularly obvious for the treated groups. However, angiogenesis or new blood vessel and hair follicles were only distinctly observed for the CSH group on the 2nd day, while these observations were relatively poorer in the other groups. In general, the results of H&E staining and MT staining all demonstrated that mature granulation and dermal tissue formed with skin appendages for wounds treated with CSH, which indicated that the CSH with cell sheets had high efficiency and high quality full-thickness skin defect repair abilities.

To investigate the cell metabolism and proliferation behaviors during skin wound healing, immunohistochemical staining for a series of

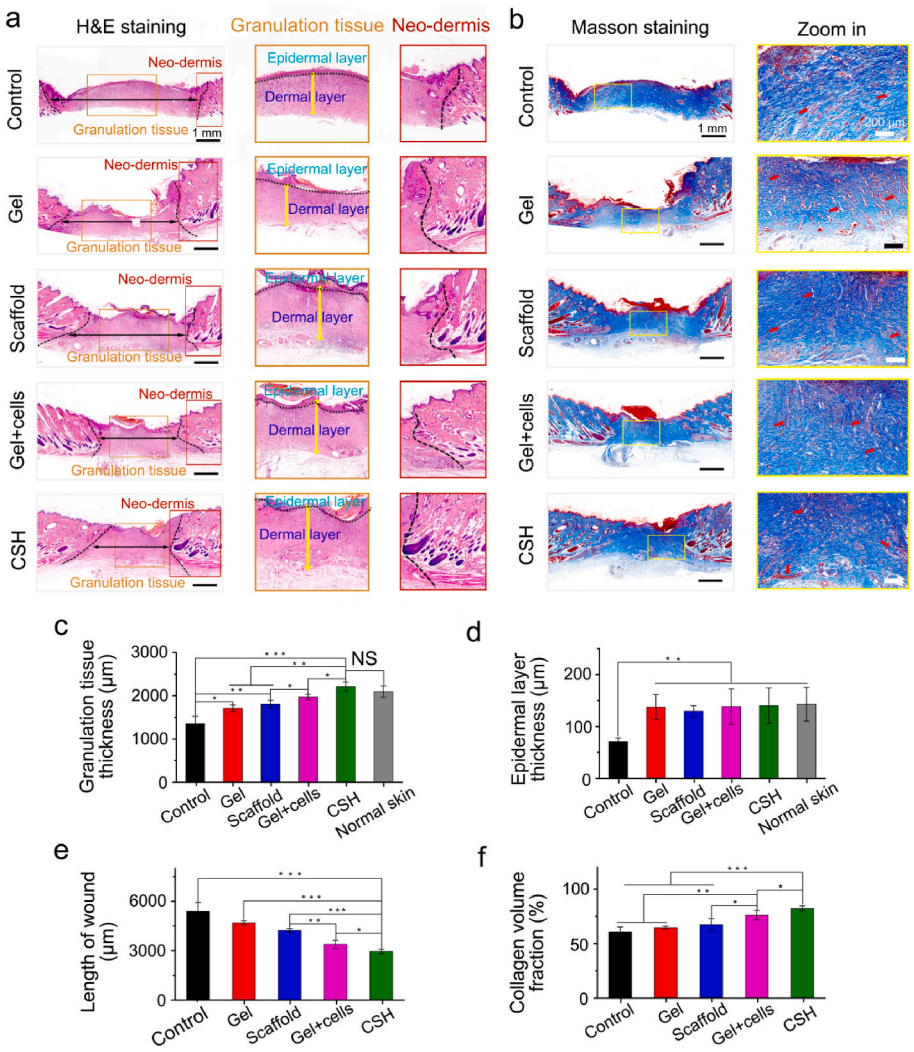

Fig. 7. Analysis of healed wounds with H&E staining and Masson staining. (a) H&E staining evaluation of wound regeneration after treatment with gel, scaffold, gel + cells, and CSH on the 10th day, the black dashed line show the border between the wound tissue and surrounding healthy skin tissue, the black dotted line label the epidermal layer; (b) Masson staining evaluation of wound regeneration after treatment with gel, scaffold, gel + cells, and CSH on the 10th day; (c) Quantification of granulation tissue thicknesses, (d) epidermal layer thickness, the thickness of the granulation tissue and epidermal layers also were compared with the normal skin, and (e) the length of wound for different treatments on the 10th day measured with H&E's trichrome stained tissue sections; (f) Quantification of collagen volume fraction for different treatments on the 10th day measured with Masson's trichrome stained tissue sections (blood vessels: red arrows), where the light blue color indicates the collagen deposition, (NS $\geq$ 0.05 , *p $<$ 0.05, **p $<$ 0.01, ***p $<$ 0.001; n = 4 in each experimental/study group; Student's *t*-test).

changes in cytokines was carried out [45]. After biomaterials are implanted *in vivo*, especially those integrated with *in vitro* cultured cells, the potential inflammatory reactions are closely related to the eventual success of the implantation procedure [46]. CD68 is ubiquitous in monocytes and pan-macrophages [47,48], and tumor necrosis factor-α (TNF-α) is a kind of typical proinflammatory factor [49], which could be a marker of inflammation [50,51]. The immunofluorescence staining of inflammation-related cytokines CD68 and TNF-α (Fig. 8a and b, and Figs. S7a and b) showed that the expression of CD68 and TNF-α are significantly lower for the treated groups, compared with those of the control group, indicating the treated groups have less inflammation. That was mainly contributed to the G-A hydrogel has a strong tissue adhesion ability and can closed the wound quickly to prevent further infection [29]. More importantly, these results indicated that there was no obvious *in vivo* rejection reaction occurred when the HSFs and HUVECs were integrated with the hydrogel and implanted into the SD rat model. Moreover, the immunofluorescence-stained of CD206 for CSH group was relatively higher than remaining groups, and the high expression of CD206 is considered to inhibit inflammation and promote tissue regeneration (Fig. 8a) [46]. In addition, immunohistochemical staining for CD31 and α-SMA for assessed angiogenesis of neo-skin, as neovascularization and vascular network formation is a sign of high-quality skin wound regeneration [6,52]. The immunofluorescence and immunohistochemical staining of angiogenesis-related cytokines CD31 and α-SMA (Fig. 8c,d, and Figs. S7c and d) showed that the expression of CD31 and α-SMA are significantly higher for the treated groups, compared with those of the control group. Notably, the CSH group obtained the highest expression of CD31 and α-SMA, which was further demonstrated the ability to promote capillary vessels and angiogenesis formation for the CSH with cell sheet. In general, these results demonstrated that mature granulation and dermis formed with skin appendages in the CSH hydrogel group, which indicated a high efficiency and quality full-thickness skin defect repairing ability.

Therefore, the one-step fabricated CSH benefitted from the advantages of the biomimetic hydrogel scaffold and cell sheets. The hydrogel scaffold provided a three-dimensional scaffold structure and biomimetic microenvironment for inducing neo-tissue ingrowth, and the integrated cell sheets maintained a superior cell viability, good intercellular connections, and cell function, which resulted in an amazing effect on the promotion of full-thickness wound healing, accompanied by skin-related appendages regeneration. This strategy of integrating hydrogels and cell sheets by a one-step pathway could expand the creativity and possible utilization of cell sheet technology and make it be more suitable for clinical applications. Moreover, such compositions of hydrogels and cell sheets also show potential applications for vascular remodeling, cartilage defects, and even organ manufacturing.

4. Conclusion

In this work, HSFs sheet and HUVECs sheet were harvested with a G-A hydrogel, and one-step integrated as cell sheet-laden hydrogel (CSH). First, *in vitro* cell tests confirmed the biocompatibility of the G-A

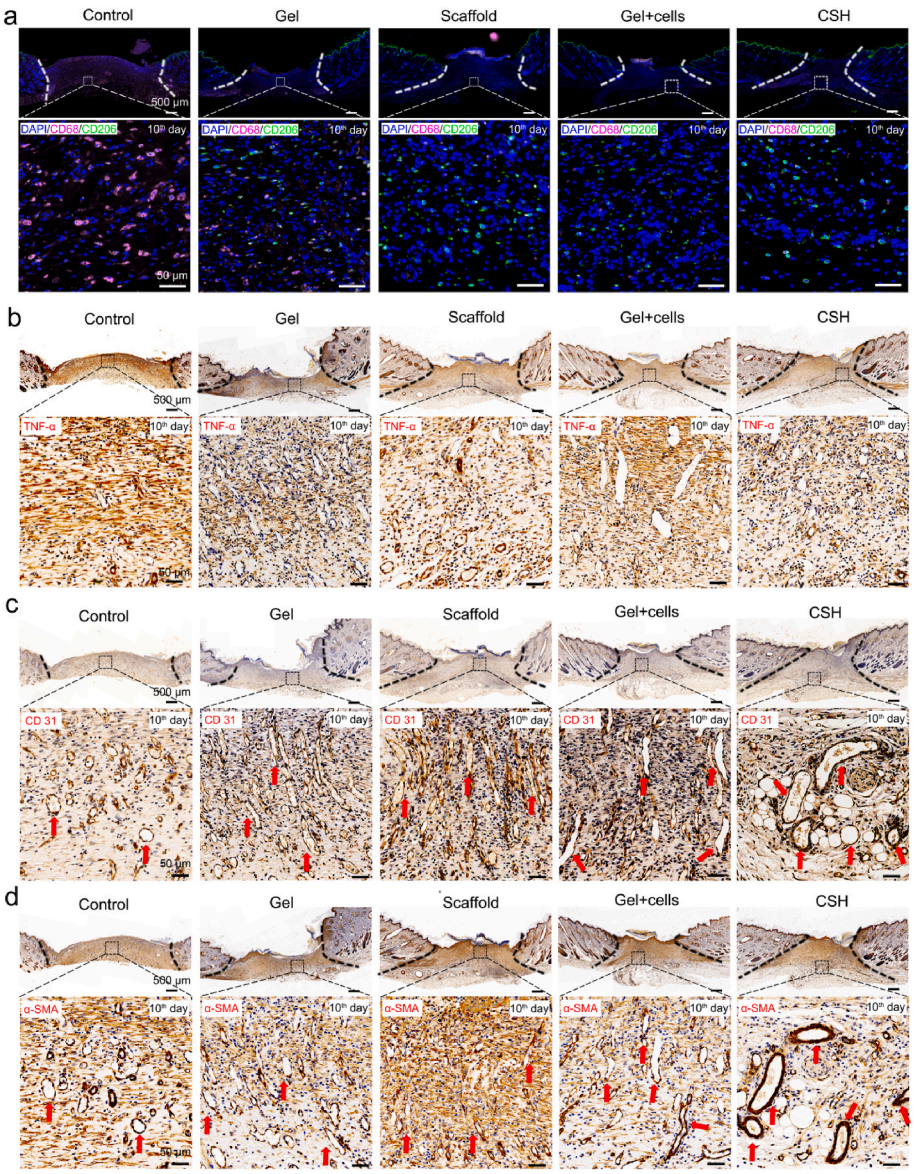

Fig. 8. Immunohistochemical staining of wound regeneration site on the 10th day after treatment. (a) Confocal images of immunofluorescence-stained control, gel, scaffold, gel + cells, and CSH. Cell nuclei are stained with DAPI (blue). Pink fluorescence corresponds to the expression of CD68 macrophages. Green fluorescence corresponds to the expression of CD206 macrophages (scale bar: 50 μm); (b) Immunostained for TNF-α on the 10th day; (c) Immunostained for CD31 on the 10th day, the red arrow indicates the vascular networks with endothelial cells; (d) Immunostained for α-SMA on the 10th day, the red arrow indicates the vascular networks with smooth muscle cells.

hydrogel. The G-A hydrogel was proven to be very suitable for integrating and harvesting the cell sheet. Moreover, the harvested cell sheet maintained a good morphology and function, and the cells had an excellent proliferation capacity and could migrate inside the hydrogel. Finally, an SD rat mouse full-thickness dorsal skin defect model was constructed, and the fabricated CSH exhibited an ideal wound healing effect within 14 days. The results of H&E staining, MT staining, and immunohistochemical staining demonstrated that the neo-skin formed with skin appendages (hair follicle, blood vessels, etc.). This project provides new insight into the utilization of cell sheets for skin regeneration, and shows clinical applications potentials.

Ethics approval and consent to participate

All the animal experiments were approved by the Ethics Committee of Sir Run Shaw Hospital, Zhejiang University.

CRediT authorship contribution statement

Huijuan Wang: Methodology, Investigation, Resources, Formal analysis, Writing – review & editing. **Deshun Sun:** Conceptualization, Methodology, Writing – review & editing. **Weiming Lin:** Methodology, Investigation. **Chao Fang:** Methodology, Investigation. **Kui Cheng:** Methodology, Resources. **Zhengzhou Pan:** Methodology, Investigation**Daping Wang:** Conceptualization, Project administration, Writing – review & editing. **Zhangfa Song:** Conceptualization, Funding acquisition, Project administration, Writing – review & editing. **Xiaojun Long:** Conceptualization, Funding acquisition, Methodology, Investigation, Resources, Data curation, Formal analysis, Writing – original draft, Writing – review & editing.

Declaration of competing interest

The authors declare that they have no known competing financial interests or personal relationships that could have appeared to influence the work reported in this paper.

Acknowledgements

This work is supported by the Shenzhen Basic Research Project Natural Science Foundation (JCYJ20210324103210027), the National Natural Science Foundation of China (No.81771502 and 82273265) and

the Department of Health of Zhejiang Province (No. 2018KY473), PhD Basic Research Initiation Project (RCBS20200714114856171).

Appendix A. Supplementary data

Supplementary data to this article can be found online at https://doi.org/10.1016/j.bioactmat.2023.06.005.

References

[1] D.R. Griffin, M.M. Archang, C.H. Kuan, W.M. Weaver, J.S. Weinstein, A.C. Feng, A. Ruccia, E. Sideris, V. Ragkousis, J. Koh, M.V. Plikus, D. Di Carlo, T. Segura, P. O. Scumpia, Activating an adaptive immune response from a hydrogel scaffold imparts regenerative wound healing, Nat. Mater. 4 (2020) 560, https://doi.org/10.1038/s41563-020-00844-w.

[2] Y. Liang, X. Zhao, T. Hu, B. Chen, Z. Yin, P.X. Ma, B. Guo, Adhesive hemostatic conducting injectable composite hydrogels with sustained drug release and photothermal antibacterial activity to promote full-thickness skin regeneration during wound healing, Small 15 (2019), e1900046, https://doi.org/10.1002/smll.201900046.

[3] M. Farokhi, F. Mottaghitalab, Y. Fatahi, A. Khademhosseini, D.L. Kaplan, Overview of silk fibroin use in wound dressings, Trends Biotechnol. 36 (2018) 907–922, https://doi.org/10.1016/j.tibtech.2018.04.004.

[4] L.A. DiPietro, Angiogenesis and scar formation in healing wounds, Curr. Opin. Rheumatol. 25 (2013) 87–91, https://doi.org/10.1097/BOR.0b013e32835b13b6.

[5] M. Ito, Y. Liu, Z. Yang, J. Nguyen, F. Liang, R.J. Morris, G. Cotsarelis, Stem cells in the hair follicle bulge contribute to wound repair but not to homeostasis of the epidermis, Nat. Med. 11 (2005) 1351–1354, https://doi.org/10.1038/nm1328.

[6] F. Zhou, Y. Hong, R. Liang, X. Zhang, Y. Liao, D. Jiang, J. Zhang, Z. Sheng, C. Xie, Z. Peng, X. Zhuang, V. Bunpetch, Y. Zou, W. Huang, Q. Zhang, E.V. Alakpa, S. Zhang, H. Ouyang, Rapid printing of bio-inspired 3D tissue constructs for skin regeneration, Biomaterials 258 (2020), 120287, https://doi.org/10.1016/j.biomaterials.2020.120287.

[7] S. MacNeil, Progress and opportunities for tissue-engineered skin, Nature 445 (2007) 874–880, https://doi.org/10.1038/nature05664.

[8] S. Jiang, J. Deng, Y. Jin, B. Qian, W. Lv, Q. Zhou, E. Mei, R.E. Neisiany, Y. Liu, Z. You, J. Pan, Breathable, antifreezing, mechanically skin-like hydrogel textile wound dressings with dual antibacterial mechanisms, Bioact. Mater. 21 (2023) 313–323, https://doi.org/10.1016/j.bioactmat.2022.08.014.

[9] I. Khan, M.N. Siddiqui, F. Jameel, R.E. Qazi, A. Salim, S. Aslam, M.B. Zaidi, Potential of stem cell seeded three-dimensional scaffold for regeneration of full-thickness skin wounds, Interface Focus 12 (2022), 20220017, https://doi.org/10.1098/rsfs.2022.0017.

[10] C. Ghobril, M.W. Grinstaff, The chemistry and engineering of polymeric hydrogel adhesives for wound closure: a tutorial, Chem. Soc. Rev. 44 (2015) 1820–1835, https://doi.org/10.1039/c4cs00332b.

[11] R. Ramakrishnan, D. Chouhan, H. Vijayakumar Sreelatha, S. Arumugam, B. B. Mandal, L.K. Krishnan, Silk fibroin-based bioengineered scaffold for enabling hemostasis and skin regeneration of critical-size full-thickness heat-induced burn wounds, ACS Biomater. Sci. Eng. 8 (2022) 3856–3870, https://doi.org/10.1021/acsbiomaterials.2c00328.

[12] Y. Guo, J. Bae, Z. Fang, P. Li, F. Zhao, G. Yu, Hydrogels and hydrogel-derived materials for energy and water sustainability, Chem. Rev. 120 (2020) 7642–7707, https://doi.org/10.1021/acs.chemrev.0c00345.

[13] D.R. Griffin, W.M. Weaver, P.O. Scumpia, D. Di Carlo, T. Segura, Accelerated wound healing by injectable microporous gel scaffolds assembled from annealed building blocks, Nat. Mater. 14 (2015) 737–744, https://doi.org/10.1038/NMAT4294.

[14] Z. Shen, Y. Cao, M. Li, Y. Yan, R. Cheng, Y. Zhao, Q. Shao, J. Wang, S. Sang, Construction of tissue-engineered skin with rete ridges using co-network hydrogels of gelatin methacrylated and poly(ethylene glycol) diacrylate, Mater. Sci. Eng. C. Mater. Biol. Appl. 129 (2021), 112360, https://doi.org/10.1016/j.msec.2021.112360.

[15] S.D. Wu, N.T. Dai, C.Y. Liao, L.Y. Kang, Y.W. Tseng, S.H. Hsu, Planar-/curvilinear-bioprinted tri-cell-laden hydrogel for healing irregular chronic wounds, Adv. Healthcare Mater. 11 (2022), 2201021, https://doi.org/10.1002/adhm.202201021.

[16] H.J. Park, Y. Zhang, S.P. Georgescu, K.L. Johnson, D. Kong, J.B. Galper, Human umbilical vein endothelial cells and human dermal microvascular endothelial cells offer new insights into the relationship between lipid metabolism and angiogenesis, Stem Cell Rev. 2 (2006) 1558–6804, https://doi.org/10.1007/s12015-006-0015-x.

[17] M. Bacakova, J. Pajorova, A. Broz, D. Hadraba, F. Lopot, A. Zavadakova, L. Vistejnova, M. Beno, I. Kostic, V. Jencova, L. Bacakova, A two-layer skin construct consisting of a collagen hydrogel reinforced by a fibrin-coated polylactide nanofibrous membrane, Int. J. Nanomed. 14 (2019) 5033–5050, https://doi.org/10.2147/IJN.S200782.

[18] Y. Hong, M. Yu, W. Weng, K. Cheng, H. Wang, J. Lin, Light-induced cell detachment for cell sheet technology, Biomaterials 34 (2013) 11–18, https://doi.org/10.1016/j.biomaterials.2012.09.043.

[19] J.A. Park, Y. Youm, H.R. Lee, Y. Lee, S.L. Barron, T. Kwak, G.T. Park, Y.C. Song, R. M. Owens, J.H. Kim, S. Jung, Transfer-tattoo-like cell-sheet delivery induced by interfacial cell migration, Adv. Mater. (2022), e2204390, https://doi.org/10.1002/adma.202204390.

[20] M.T. Cerqueira, R.P. Pirraco, A.R. Martins, T.C. Santos, R.L. Reis, A.P. Marques, Cell sheet technology-driven re-epithelialization and neovascularization of skin wounds, Acta Biomater. 10 (2014) 3145–3155, https://doi.org/10.1016/j.actbio.2014.03.006.

[21] J.L. Roh, J. Lee, E.H. Kim, D. Shin, Plasticity of oral mucosal cell sheets for accelerated and scarless skin wound healing, Oral Oncol. 75 (2017) 81–88, https://doi.org/10.1016/j.oraloncology.2017.10.024.

[22] Y.C. Lin, T. Grahovac, S.J. Oh, M. Ieraci, J.P. Rubin, K.G. Marra, Evaluation of a multi-layer adipose-derived stem cell sheet in a full-thickness wound healing model, Acta Biomater. 9 (2013) 5243–5250, https://doi.org/10.1016/j.actbio.2012.09.028.

[23] S.W. Kim, G.B. Im, G.J. Jeong, S. Baik, J. Hyun, Y.J. Kim, C. Pang, Y.C. Jang, S. H. Bhang, Delivery of a spheroids-incorporated human dermal fibroblast sheet increases angiogenesis and M2 polarization for wound healing, Biomaterials 275 (2021), 120954, https://doi.org/10.1016/j.biomaterials.2021.120954.

[24] G. Pan, Q. Guo, Y. Ma, H. Yang, B. Li, Thermo-responsive hydrogel layers imprinted with RGDS peptide: a system for harvesting cell sheets, Angew Chem. Int. Ed. Engl. 52 (2013) 6907–6911, https://doi.org/10.1002/anie.201300733.

[25] X. Long, Y. Yi, X. Wang, X. Duan, Y. Sun, C. Wu, W. Weng, B. Xu, K. Cheng, H. Wang, J. Lin, Gr/TiO_2 films with light-controlled positive/negative charge for cell harvesting application, ACS Biomater. Sci. Eng. 6 (2020) 2020–2028, https://doi.org/10.1021/acsbiomaterials.9b01946.

[26] H. Akiyama, A. Ito, Y. Kawabe, M. Kamihira, Genetically engineered angiogenic cell sheets using magnetic force-based gene delivery and tissue fabrication techniques, Biomaterials 31 (2010) 1251–1259, https://doi.org/10.1016/j.biomaterials.2009.11.017.

[27] K.M. Persson, R. Karlsson, K. Svennersten, S. Löffler, E.W.H. Jager, A. Richter-Dahlfors, P. Konradsson, M. Berggren, Electronic control of cell detachment using a self-doped conducting polymer, Adv. Mater. 23 (2011) 4403–4408, https://doi.org/10.1002/adma.201101724.

[28] Y. Zhu, Y. Liao, Y. Zhang, M.I. Shekh, J. Zhang, Z. You, B. Du, C. Lian, Q. He, Novel nanofibrous membrane-supporting stem cell sheets for plasmid delivery and cell activation to accelerate wound healing, Bioeng. Transl. Med. 7 (2022), e10244, https://doi.org/10.1002/btm2.10244.

[29] X. Long, X. Xu, D. Sun, Y. Hong, C. Wen, Y. Xie, B. Yan, H. Zhang, Q. Ge, W. Li, L. Duan, H. Ouyang, D. Wang, Biomimetic macroporous hydrogel with a triple-network structure for full-thickness skin regeneration, Appl. Mater. Today 27 (2022), 101442, https://doi.org/10.1016/j.apmt.2022.101442.

[30] Y. Zhang, C. Li, Q. Zhu, R. Liang, C. Xie, S. Zhang, Y. Hong, H. Ouyang, A long-term retaining molecular coating for corneal regeneration, Bioact. Mater. 6 (2021) 4447–4454, https://doi.org/10.1016/j.bioactmat.2021.04.032.

[31] W. Liu, W. Ou-Yang, C. Zhang, Q. Wang, X. Pan, P. Huang, C. Zhang, Y. Li, D. Kong, W. Wang, Staphylococcus aureus-synthetic polymeric antibacterial hydrogel for methicillin-resistant infected wound healing: nanoantimicrobial self-assembly, drug- and cytokine-free strategy, ACS Nano 14 (2020) 12905–12917, https://doi.org/10.1021/acsnano.0c03855.

[32] X. Wang, C. Yao, W. Weng, K. Cheng, Q. Wang, Visible-light-responsive surfaces for efficient, noninvasive cell sheet harvesting, ACS Appl. Mater. Interfaces 9 (2017) 28250–28259, https://doi.org/10.1021/acsami.7b08868.

[33] J. You, J.S. Heo, J. Kim, T. Park, B. Kim, H.S. Kim, Y. Choi, H.O. Kim, E. Kim, Noninvasive photodetachment of stem cells on tunable conductive polymer nano thin films: selective harvesting and preserved differentiation capacity, ACS Nano 7 (2013) 4119–4128, https://doi.org/10.1021/nn400405t.

[34] K. Yue, G. Trujillo-de Santiago, M.M. Alvarez, A. Tamayol, N. Annabi, A. Khademhosseini, Synthesis, properties, and biomedical applications of gelatin methacryloyl (GelMA) hydrogels, Biomaterials 73 (2015) 254–271, https://doi.org/10.1016/j.biomaterials.2015.08.045.

[35] L. Han, X. Lu, K. Liu, K. Wang, L. Fang, L.T. Weng, H. Zhang, Y. Tang, F. Ren, C. Zhao, G. Sun, R. Liang, Z. Li, Mussel-inspired adhesive and tough hydrogel based on nanoclay confined dopamine polymerization, ACS Nano 11 (2017) 2561–2574, https://doi.org/10.1021/acsnano.6b05318.

[36] D. Cai, Y. Yang, J. Lu, Z. Yuan, Y. Zhang, X. Yang, X. Huang, T. Li, X. Tian, B. Xu, P. Wang, H. Lei, Injectable carrier-free hydrogel dressing with anti-multidrug-resistant staphylococcus aureus and anti-inflammatory capabilities for accelerated wound healing, ACS Appl. Mater. Interfaces 14 (2022) 43035–43049, https://doi.org/10.1021/acsami.2c15463.

[37] N. Karimi Khorrami, M. Radi, S. Amiri, D.J. McClements, Fabrication and characterization of alginate-based films functionalized with nanostructured lipid carriers, Int. J. Biol. Macromol. 182 (2021) 373–384, https://doi.org/10.1016/j.ijbiomac.2021.03.159.

[38] L. Dou, B. Li, K. Zhang, X. Chu, H. Hou, Physical properties and antioxidant activity of gelatin-sodium alginate edible films with tea polyphenols, Int. J. Biol. Macromol. 118 (2018) 1377–13783, https://doi.org/10.1016/j.ijbiomac.2018.06.121.

[39] Y. Yang, J. Zhang, Z. Liu, Q. Lin, X. Liu, C. Bao, Y. Wang, L. Zhu, Tissue-integratable and biocompatible photogelation by the imine crosslinking reaction, Adv. Mater. 28 (2016) 2724–2730, https://doi.org/10.1002/adma.201505336.

[40] Y. Hong, F. Zhou, Y. Hua, X. Zhang, C. Ni, D. Pan, Y. Zhang, D. Jiang, L. Yang, Q. Lin, Y. Zou, D. Yu, D.E. Arnot, X. Zou, L. Zhu, S. Zhang, H. Ouyang, A strongly adhesive hemostatic hydrogel for the repair of arterial and heart bleeds, Nat. Commun. 10 (2019) 2060, https://doi.org/10.1038/s41467-019-10004-7.

[41] H. Inada, M. Udono, K. Matsuda-Ito, K. Horisawa, Y. Ohkawa, S. Miura, T. Goya, J. Yamamoto, M. Nagasaki, K. Ueno, D. Saitou, M. Suyama, Y. Maehara, W. Kumamaru, Y. Ogawa, S. Sekiya, A. Suzuki, Direct reprogramming of human

umbilical vein- and peripheral blood-derived endothelial cells into hepatic progenitor cells, Nat. Commun. 11 (2020) 5292, https://doi.org/10.1038/s41467-020-19041-z.

[42] M. Kitada, T. Murakami, S. Wakao, G. Li, M. Dezawa, Direct conversion of adult human skin fibroblasts into functional Schwann cells that achieve robust recovery of the severed peripheral nerve in rats, Glia 67 (2019) 950–966, https://doi.org/10.1002/glia.23582.

[43] Z. Wu, Y. Hong, Combination of the silver-ethylene interaction and 3D printing to develop antibacterial superporous hydrogels for wound management, ACS Appl. Mater. Interfaces 11 (2019) 33734–33747, https://doi.org/10.1021/acsami.9b14090.

[44] S. Lu, X. Zhang, Z. Tang, H. Xiao, M. Zhang, K. Liu, L. Chen, L. Huang, Y. Ni, H. Wu, Mussel-inspired blue-light-activated cellulose-based adhesive hydrogel with fast gelation, rapid haemostasis and antibacterial property for wound healing, Chem. Eng. J. 417 (2021), 129329, https://doi.org/10.1016/j.cej.2021.129329.

[45] X. Kong, J. Fu, K. Shao, L. Wang, X. Lan, J. Shi, Biomimetic hydrogel for rapid and scar-free healing of skin wounds inspired by the healing process of oral mucosa, Acta Biomater. 100 (2019) 255–269, https://doi.org/10.1016/j.actbio.2019.10.011.

[46] Q. Zhu, Y. Hong, Y. Huang, Y. Zhang, C. Xie, R. Liang, C. Li, T. Zhang, H. Wu, J. Ye, X. Zhang, S. Zhang, X. Zou, H. Ouyang, Polyglutamic acid-based elastic and tough adhesive patch promotes tissue regeneration through in situ macrophage modulation, Adv. Sci. 9 (2022), 2106115, https://doi.org/10.1002/advs.202106115.

[47] J. Qu, X. Zhao, Y. Liang, T. Zhang, P.X. Ma, B. Guo, Antibacterial adhesive injectable hydrogels with rapid self-healing, extensibility and compressibility as wound dressing for joints skin wound healing, Biomaterials 183 (2018) 185–199, https://doi.org/10.1016/j.biomaterials.2018.08.044.

[48] Y. Huang, L. Mu, X. Zhao, Y. Han, B. Guo, Bacterial growth-induced tobramycin smart release self-healing hydrogel for pseudomonas aeruginosa-infected burn wound healing, ACS Nano 16 (2022) 13022–13036, https://doi.org/10.1021/acsnano.2c05557.

[49] R. Yu, M. Li, Z. Li, G. Pan, Y. Liang, B. Guo, Supramolecular thermo-contracting adhesive hydrogel with self-removability simultaneously enhancing noninvasive wound closure and MRSA-infected wound healing, Adv. Healthc. Mater. 11 (2022), 2102749, https://doi.org/10.1002/adhm.202102749.

[50] Y. Yang, Y. Liang, J. Chen, X. Duan, B. Guo, Mussel-inspired adhesive antioxidant antibacterial hemostatic composite hydrogel wound dressing via photo-polymerization for infected skin wound healing, Bioact. Mater. 8 (2022) 341–354, https://doi.org/10.1016/j.bioactmat.2021.06.014.

[51] S. Li, Q. Dong, X. Peng, Y. Chen, H. Yang, W. Xu, Y. Zhao, P. Xiao, Y. Zhou, Self-healing hyaluronic acid nanocomposite hydrogels with platelet-rich plasma impregnated for skin regeneration, ACS Nano 16 (2022) 11346–11359, https://doi.org/10.1021/acsnano.2c05069.

[52] M. Wang, C. Wang, M. Chen, Y. Xi, W. Cheng, C. Mao, T. Xu, X. Zhang, C. Lin, W. Gao, Y. Guo, B. Lei, Efficient angiogenesis-based diabetic wound healing/skin reconstruction through bioactive antibacterial adhesive ultraviolet shielding nanodressing with exosome release, ACS Nano 13 (2019) 10279–10293, https://doi.org/10.1021/acsnano.9b03656.